



Planetary scale selection of the Madden–Julian Oscillation in an air-sea coupled dynamic moisture model

Yuntao Wei^{1,2,5} · Fei Liu³ · Mu Mu^{1,4} · Hong-Li Ren⁵

Received: 25 December 2016 / Accepted: 16 July 2017 / Published online: 21 July 2017
© Springer-Verlag GmbH Germany 2017

Abstract The authors present an air–sea coupled dynamic moisture (ASDM) model to explore the mechanism of preferred planetary scale of the Madden–Julian Oscillation (MJO). This ASDM model, extended from the original frictionally coupled dynamic moisture model and a mixed layer model, can present a good simulation of planetary-scale characteristics of the MJO, including a slow eastward propagation of 5 m s^{-1} , coupled Rossby–Kelvin wave-like structure, and phase leading of convective center by warm sea surface temperature (SST). It is interesting that the planetary-scale selection in terms of instability is only found in the nonlinear ASDM model with the assumption of positive-only heating. Such a scale selection, however, cannot be found in the ASDM model with linear heating or in an uncoupled atmosphere model. The essential mechanism for the scale selection is nonlinear positive-only heating, and the air-sea interaction primarily provides

an instability source to support this scale selection. This scale selection is attributed to different phase speeds of coupled moist Rossby–Kelvin waves and dry Kelvin waves. From short-wave initial perturbations, the easterly wind anomalies of eastward-propagating dry Kelvin waves from a stronger wave component will catch up with other weaker moist components and suppress their westerly wind anomalies, resulting in weak SST gradient as well as reduced moisture convergence and precipitation for these suppressed components. As a result, the wavenumber-one structure is selected. The Warm Pool-like mean state will select the stronger component among the initial short-wave perturbations and accelerate this scale selection process. These results provide new insight into MJO mechanism in terms of air-sea interaction.

Keywords MJO · Air–sea interaction · Positive-only heating · Planetary-scale selection · Coupled Kelvin–Rossby waves · Warm Pool

✉ Fei Liu
liuf@nuist.edu.cn

¹ Key Laboratory of Ocean Circulation and Waves, Institute of Oceanology, Chinese Academy of Sciences, Qingdao 266071, China

² University of Chinese Academy of Sciences, Beijing 100049, China

³ Earth System Modeling Center and Climate Dynamics Research Center, Nanjing University of Information Science and Technology, Nanjing 210044, China

⁴ Laboratory for Ocean and Climate Dynamics, Qingdao National Laboratory for Marine Science and Technology, Qingdao 266237, China

⁵ Laboratory for Climate Studies & CMA-NJU Joint Laboratory for Climate Prediction Studies, National Climate Center, China Meteorological Administration, Beijing 100081, China

1 Introduction

The Madden–Julian Oscillation (MJO; Madden and Julian 1971, 1972) is a dominant intraseasonal mode in the tropics, and it is well distinguished from other moist equatorial waves (Wheeler and Kiladis 1999; Kiladis et al. 2009). The MJO is often featured by (1) zonal planetary scale (Madden and Julian 1972, 1994; Zhang 2005), (2) slow (fast) eastward propagation of 5 m s^{-1} (15 m s^{-1}) and developing (decaying) across the Eastern (Western) Hemisphere (Hendon and Salby 1994; Knutson et al. 1986), and (3) an equatorially trapped, coupled Kelvin–Rossby wave structure, with low pressure and easterly wind anomalies to the east of the main convective precipitation and two cyclones on

both sides of the equator to the west (Rui and Wang 1990; Wang and Rui 1990; Kang et al. 2013; Adames and Wallace 2014). Recently, a frictionally coupled dynamic moisture (FCDM) model was developed by Wang and Chen (2016) and Liu and Wang (2016a, b), which involves tri-interaction among convective heating, moisture, and wave–planetary boundary layer (PBL) dynamics, and can well simulate the aforementioned MJO characteristics when the planetary-scale initiation is specified. The physical processes discussed in these studies, however, are confined to the atmosphere only.

The MJO, however, is more than a pure atmospheric perturbation. A large number of MJO studies using observations, simulations, and theoretical analysis revealed the crucial importance of atmosphere–ocean coupling in triggering the MJO (Li et al. 2008; Miura et al. 2009; Seiki et al. 2015), maintaining the MJO (e.g., Zhang 1996; Lau and Sui 1997; Waliser et al. 1999; Sobel and Gildor 2003; Maloney and Sobel 2007; De Szeoke et al. 2015; Fu et al. 2015; DeMott et al. 2016), and even causing different propagations of the MJO (Flatau et al. 1997; Fu et al. 2003; Inness and Slingo 2003; Hsu and Li 2012; DeMott et al. 2014). These roles of air-sea interaction in MJO dynamics have been well reviewed in two recent review papers (Li 2014; DeMott et al. 2015).

Some literatures suggested that atmosphere–ocean thermodynamic coupling plays a critical role in terms of MJO instability, especially its scale selection. For example, Wang and Xie (1998) developed an idealized linear atmosphere–ocean coupling framework and showed that it is the coaction of wind and mixed layer, namely, the wind-evaporation-entrainment feedback, that destabilizes the neutral wave-conditional instability of the second kind (CISK), while the cloud-sea surface temperature (SST) feedback represented by short-wave radiation and oceanic wave dynamics is of secondary importance. By coupling this mixed layer model with a neutral atmospheric MJO skeleton model (Majda and Stechmann 2009), the effect of the wind-mixed layer thermodynamic coaction was confirmed by Liu and Wang (2013), which showed that this mechanism can select preferred eastward-moving wavenumber-one MJO-like mode, although the cloud-SST feedback contributes to both eastward and westward propagations. They also showed that this kind of instability was only generated under the background westerly wind. These results indicate the crucial importance of atmosphere–ocean coupling in regulating the MJO. Thus, it is necessary to include the air-sea interaction in the FCDM model.

To understand the MJO dynamics, the primary scientific questions to be firstly solved are why and how the MJO always exhibits a preferred planetary-scale packet. On this scale selection issue, there have been several theories. For example, when extended by using a positive-only cumulus

parameterization scheme, the wave-CISK model can simulate the most unstable Kelvin wave at zonal wavenumber one (Lau and Peng 1987; Lim et al. 1990; Wang and Xue 1992). The PBL moisture convergence can also select the planetary wave as the most unstable mode in the frictional MJO skeleton model (Liu and Wang 2012). One interesting MJO theory, the so-called “moisture mode” theory (Sobel and Maloney 2012, 2013), exhibits dramatically a zonal wavenumber dependence in terms of cloud-radiation feedback, with the largest growth rate on the planetary scale (Adames and Kim 2016). The recently developed FCDM model also simulates the most unstable zonal wavenumber-one MJO mode (Liu and Wang 2016a, b; Wang and Chen 2016; Wang et al. 2016). Li and Zhou (2009) explained this planetary-scale selection by using a two and a half layer atmosphere model, and suggested that this scale selection is caused by nonlinear positive-only heating. For shorter waves, the smaller distance of one wet component with another allows the interference between the faster dry waves and the slower wet coupled Rossby–Kelvin waves, which largely prevents the development of small-scale perturbation and leads to the planetary-scale selection. This positive-only heating mechanism gives us a better insight into the physical process regarding scale selection of the MJO. It is, however, still obscure on how this mechanism evolves in an air-sea coupled system and how the realistic SST pattern modulates this mechanism.

With the crucial importance of both air-sea interaction and positive-only heating to the MJO confirmed, there are still too few theoretical studies focusing on their combined effect on the MJO dynamics. Thus, we will couple the aforementioned mixed-layer model (Wang et al. 1995; Wang and Xie 1998) with the most updated FCDM model (Liu and Wang 2016a, b; Wang and Chen 2016; Wang et al. 2016) to investigate the MJO planetary-scale selection under the positive-only heating assumption.

This paper is organized as follows. The model framework and model experiments are introduced in Sect. 2. The MJO simulation and planetary-scale selection over the uniform and Warm Pool-like basic states are discussed in Sects. 3 and 4, respectively. The summary and concluding remarks are given in Sect. 5.

2 Model framework and analysis methods

2.1 Model formulations

The theoretical model used here is the air-sea coupled dynamic moisture (ASDM) model, which is built using the original FCDM model proposed by Wang and Chen (2016) and Liu and Wang (2016a, b) for the MJO and a simple oceanic mixed-layer model proposed by Wang et al. (1995)

and Wang and Xie (1998). The FCDM model is extended from the Matsuno–Gill model (Matsuno 1966; Gill 1980) by using an idealized Betts–Miller cumulus parameterization (Betts 1986; Betts and Miller 1986), which includes trio-interaction among convective heating, moisture, and wave-PBL dynamics. The FCDM model includes both tropical wave dynamics and moisture processes, which can simulate robust large-scale characteristics of the observed MJO, including slow eastward propagation, planetary-scale circulation, and wavenumber-independent dispersion relationship (Liu and Wang 2016a). In this simple ASDM model, the lower troposphere will become moist and warm through some SST feedbacks (Philander et al. 1984; Hirst 1986; Zebiak 1986; Davey and Gill 1987; Lindzen and Nigam 1987).

To describe motion in the free troposphere over the tropics, we use the simplest form of an one and a half layer atmosphere mode (Wang 1988b; Wang and Chen 2016). The seasonal-mean moisture advection and the PBL dynamics are also removed to isolate the influence of air-sea coupling. Thus, on an equatorial β -plane in p coordinate, the model equations in terms of the gravest baroclinic mode can be formulated as follows:

$$U_t - \beta y V = -\phi_x - \varepsilon_a U, \quad (1a)$$

$$V_t + \beta y U = -\phi_y - \varepsilon_a V, \quad (1b)$$

$$\phi_t + C_a^2 D = -\gamma L_C P_r - \gamma \eta_T T - \mu_a \phi, \quad (1c)$$

$$q_t + \Delta p / g \bar{q}_3 D = -P_r + \eta_E / L_C T, \quad (1d)$$

where the prognostic variables U , V , ϕ , and q denote, respectively, the low-level zonal wind, meridional wind, geopotential height, and specific humidity anomalies. β measures the role of planet curvature change on the equator. ε_a and μ_a are damping coefficients used in the momentum and thermodynamic equations, which denote atmospheric Rayleigh friction and Newtonian cooling, respectively. The tropospheric damping is neglected in this work except in the damping sensitivity experiments. C_a is the dry gravity wave speed. L_C is the condensational latent heating. η_T and η_E are the SST forcing and latent heating coefficients, respectively. \bar{q}_3 is the seasonal-mean low-level specific humidity. Δp and g are tropospheric depth and gravity acceleration, respectively. The interactive convective heating is parameterized by precipitation P_r . T is SST or mixed-layer temperature. D is lower-tropospheric wave divergence. $\gamma = Rg/2C_p p_2$ is the proportional constant, in which R , C_p , and p_2 are the specific gas constant, the specific heat capacity, and mid-tropospheric height, respectively.

The ocean model used here is a mixed-layer model, which is distilled from the atmosphere–ocean coupled model developed by Wang et al. (1995) and Wang and Xie (1998). When neglecting the oceanic wave dynamics,

the penetrating solar radiation flux at the mixed-layer base, SST advection, and horizontally-varying buoyancy, the linearized upper-ocean model can be written as follows:

$$h_{1t} = E_M \bar{U} U + \bar{w}_e (3U/\bar{U} - H/H_1 H_2 h_1), \quad (2a)$$

$$T_t = D_{rad} D - D_{ent} (3U/\bar{U} - h_1/H_1) - D_{eva} U/\bar{U} - \mu_o T, \quad (2b)$$

where h_1 is mixed-layer depth, E_M is the Ekman pumping coefficient, \bar{U} is the background surface zonal wind, and \bar{w}_e is the mean entrainment rate at the mixed-layer base. H and H_1 are, respectively, the background thermocline and mixed-layer depth, and $H_2 = H - H_1$. The terms D_{rad} , D_{ent} , and D_{eva} denote the coefficients of the cloud-SST, wind-entrainment, and evaporation feedbacks, respectively. Equation (2b) suggests that the essential processes determining the SST tendency are the cloud-radiation feedback, the wind-entrainment feedback, and the evaporation feedback, which are proportional to the low-level wave convergence and zonal wind perturbations. The definitions of the model parameters used in this paper are listed in Table 1.

Table 1 Summary of model parameters used in this paper

Parameter	Description	Default value
ε_a	Coefficient of Rayleigh friction	0
μ_a	Coefficient of Newtonian cooling	0
C_a	Speed of dry gravity wave	50 m s ⁻¹
η_T	SST forcing coefficient	12 kg s ⁻³ K ⁻³
η_E	Latent heating coefficient	12 kg s ⁻³ K ⁻³
Δp	Tropospheric depth	400 hPa
p_2	Mid-tropospheric height	500 hPa
p_s	Surface pressure	1000 hPa
R	Specific gas constant	287 J K ⁻¹ kg ⁻¹
C_p	Specific heating at constant pressure	1004 J K ⁻¹ kg ⁻¹
g	Gravity acceleration	9.8 m s ⁻²
E_M	Ekman-pumping coefficient	3.0×10^{-7} s ⁻¹
\bar{U}	Mean surface zonal wind	3.0 m s ⁻¹
\bar{w}_e	Mean entrainment rate at mixed-layer base	2.0×10^{-6}
H	Mean thermocline depth	150 m
H_1	Mean mixed-layer depth	40 m
D_{rad}	Coefficient of cloud-SST feedback	0.1 K
D_{ent}	Coefficient of wind-entrainment feedback	0.9×10^{-7} K s ⁻¹
D_{eva}	Coefficient of evaporation feedback	0.72×10^{-7} K s ⁻¹
μ_o	Newtonian damping coefficient of ocean	1.0×10^{-8} s ⁻¹
m	Power exponent of moisture damping	3.45
τ	Convection relaxation time scale	2.0 h
α	Moisture reference coefficient	0.1

2.2 Basic state

The background surface specific humidity \bar{q}_s over the tropical ocean can be obtained empirically by using the following formulation (Wang 1988a):

$$\bar{q}_s(SST) = (0.94 \times SST(\text{ }^{\circ}\text{C}) - 7.64) \times 10^{-3}. \quad (3)$$

Tomasi (1984) showed that the observational absolute humidity in the tropical atmosphere over the ocean decreased upward exponentially. So, Wang (1988a) suggested the background specific humidity can be formulated by:

$$\bar{q}(p) = \bar{q}_s(p/p_s)^{m-1}, \quad (4)$$

where p_s denotes surface pressure and m is an index measuring the moisture damping. For a uniform SST of $29.5\text{ }^{\circ}\text{C}$, the lower tropospheric humidity from 825 to 500 hPa can be obtained by integrating Eq. (4): $\bar{q}_3 = \int_{825}^{500} \bar{q}_s(p/p_s)^{m-1} dp$. An idealized but nearly realistic background SST, i.e., Warm Pool-like SST, is studied here (Fig. 1a), and the associated low-level specific humidity with zonal mean removed is also shown in Fig. 1b. Both the background specific humidity and underlying SST feature the maxima on the equator and weaken poleward, while in the zonal direction the maxima are located in the Warm Pool region.

2.3 Precipitation parameterization

To close the ASDM model, the Betts–Miller precipitation scheme is specified as follows,

$$P_r = \frac{1}{\tau} \left(q + \frac{\alpha}{\gamma L_C} \phi \right), \quad (5)$$

where the first term on the r. h. s. implies that the convective available potential energy will be released, and the

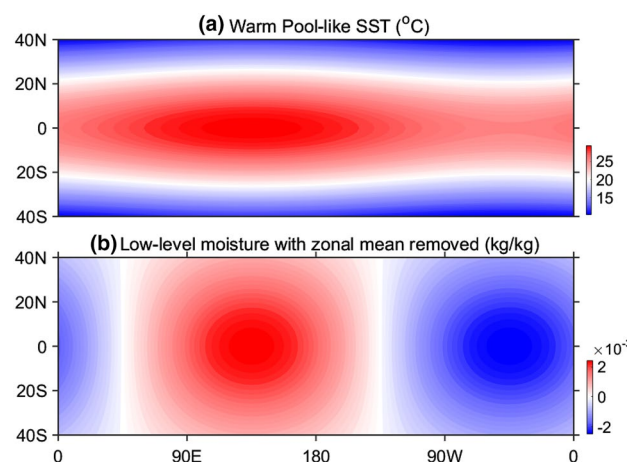


Fig. 1 Warm Pool-like basic state. **a** Background SST ($^{\circ}\text{C}$) and **b** associated low-level (825–500 hPa) specific humidity (kg kg^{-1}) with zonal mean moisture removed

second term is assumed to relax the moisture to its reference state (Wang and Chen 2016). The parameters of α and τ are also listed in Table 1. Following Betts (1986) and Wang and Chen (2016), a convective adjustment time scale (τ) of 2 h is used in the ASDM model, which means a quick moisture feedback to precipitation.

A positive-only precipitation, as used in Li and Zhou (2009), is assumed. In this case, precipitation can be calculated by

$$P_r = \frac{1}{\tau} \delta \left(q + \frac{\alpha}{\gamma L_C} \phi \right), \quad (6)$$

where δ is the heating coefficient. In the nonlinear cumulus scheme, δ is unity in the region where $q + \frac{\alpha}{\gamma L_C} \phi > 0$ and zero where $q + \frac{\alpha}{\gamma L_C} \phi \leq 0$. For the linear heating, δ is always unity.

2.4 Numerical scheme and analysis methods

A numerical method is needed to obtain solutions of this nonlinear initial and boundary value problem. The periodic and zero-flux boundary conditions are used along the zonal and meridional directions, respectively. A Kelvin wave-like initial condition in the lower troposphere is used in this work. Following Li and Zhou (2009), we specified an initial geopotential height anomaly with different wavenumbers from 1 to 15. A typical initial perturbation of zonal wavenumber four is shown in Fig. 2, in which the strength is maximum at the equator, and weakens poleward. The model domain is between 40°S and 40°N with a resolution of 2.5° by 2.5° . The forward and central difference schemes are adopted in time and space, respectively. A few sensitivity experiments using different spatial resolutions indicated that solutions are not sensitive to the grid sizes (figure not shown). A five-point space smoothing is performed every five steps.

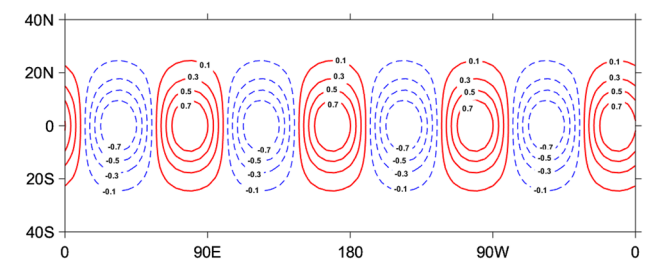


Fig. 2 A wavenumber-four Kelvin wave-like structure for the initial normalized geopotential height anomaly. The solid red (dashed blue) contours denote positive (negative) anomalies. Contour interval is 0.2 and zero contours are not shown

For all the experiments conducted in this study, linear simulations versus nonlinear simulations help reveal the role of positive-only heating. To explore planetary-scale selection of the MJO, the Fast Fourier Transform (FFT) is performed on model outputs to diagnose the evolution of individual wavenumbers. The respective contributions of the three oceanic feedbacks, namely, the cloud-radiation, wind-entrainment and evaporation feedbacks, can be isolated using this simple air-sea coupled model, which will be presented in details next.

3 Results from a uniform basic state

3.1 Simulated MJO in the ASDM model

The observed characteristics of the MJO have been well simulated in the FCDM model (Liu and Wang 2016a, b; Wang and Chen 2016; Wang et al. 2016). So, let us first make sure that the ASDM model can also simulate the observed MJO well with specified planetary-scale initiation. In this section, a globally uniform SST of 29.5 °C is used.

Figure 3 shows the time-longitude sections of the simulated precipitation and zonal wind anomalies on the equator, initiated from zonal wavenumber one, in the ASDM model with linear and nonlinear heating, respectively. In the linear ASDM model, slow eastward propagation of 6.4 m s⁻¹ is simulated for the MJO, and the low-level zonal winds are tightly coupled with convective precipitation, denoted by a phase leading of the positive convective center by anomalous easterly wind (Fig. 3a). In the nonlinear ASDM model, the slow eastward propagation is also well simulated (Fig. 3b), which has a speed of 5.4 m s⁻¹. More interestingly, a strong asymmetric structure is simulated by the nonlinear ASDM model, and its precipitation has a much smaller zonal scale than that in the linear model. In this nonlinear model, the easterly wind anomalies have much larger zonal scales than the westerly wind anomalies, while the latter have larger amplitude.

The horizontal structures of simulated MJO, initiated from wavenumber one, are shown in Fig. 4 for the linear and nonlinear models, respectively. Some observed phase relationships among different variables have been well simulated by both linear and nonlinear models. For example, a clear horizontal planetary-scale Kelvin–Rossby coupled wave structure can be seen in both panels of Fig. 4, in which low pressure and easterly wind anomalies are located to the east of main convective precipitation, and two cyclones are seen to the west on both sides of the equator. Positive SST anomalies, under the anomalous easterly wind, lead the convective center by about one quarter of the

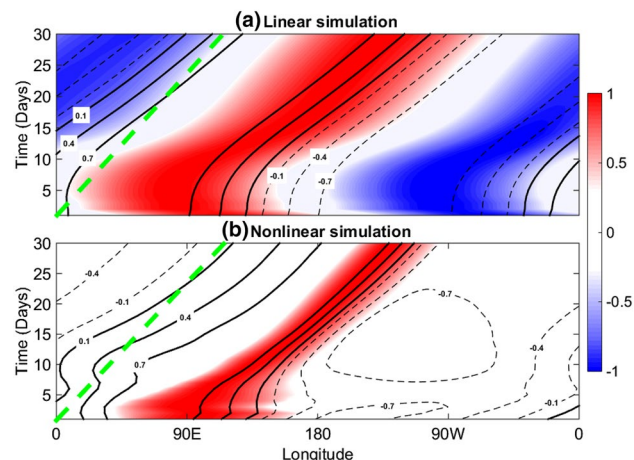


Fig. 3 Time-longitude sections of normalized low-level zonal wind (contour) and precipitation (shading) anomalies on the equator in the ASDM model under **a** linear heating and **b** nonlinear positive-only heating, in which a zonal wavenumber-one Kelvin wave-like geopotential height anomaly is used as the initial perturbation. The solid (dashed) contours denote westerly (easterly) anomalies. Contour interval is 0.3 and zero contours are not shown. Only precipitation anomalies above one third of the magnitude are shaded. The green dashed line denotes the reference speed of 5 m s⁻¹. All variables are normalized for each day, based on their magnitude on that day

cycle, which is consistent with previous studies (Wang and Xie 1998; Liu and Wang 2013).

In the linear simulation (Fig. 4a), there have positive geopotential height anomalies to the west of the positive convective center, because the negative convection anomalies can excite positive geopotential height anomalies to propagate eastward. These positive anomalies, however, disappear in the nonlinear simulation (Fig. 4b) because of lack of negative convection anomalies.

3.2 Planetary-scale selection

Reasonable MJO simulations in both linear and nonlinear ASDM models allow us to investigate the mechanism of planetary-scale selection for the MJO. Figure 5 shows different evolutions of the same initial wavenumber-four perturbation in the linear and nonlinear ASDM models. In the linear simulation, the model reaches its steady state on day 10, and the wavenumber-four convection-circulation coupled system moves eastward slowly, having a phase speed of 3.2 m s⁻¹ (Fig. 5a). The nonlinear model gives a very different simulation (Fig. 5b). For the initial wavenumber-four perturbation, the eastward propagation is very slow, and the phase speed is only 1.3 m s⁻¹. There is a transition from wavenumber four to wavenumber one from day 5 to day 30, and there is also a speed up with a speed of 8 m s⁻¹ from day 50 to day 70 after the scale-selection process. The model reaches its steady state on day 80, and the selected

Fig. 4 Horizontal structures of simulated MJO in the ASDM model initiated from the wavenumber one perturbation. Shown are the precipitation (thick contour), low-level geopotential height (thin contour), low-level wind (vector), and SST (shading) anomalies at day 30 in the simulations with **a** linear heating and **b** nonlinear positive-only heating. Each field is normalized by its magnitude. The solid (dashed) contours indicate positive (negative) anomalies. For the geopotential height anomalies, contour interval is 0.2 and zero contours are not shown. Only precipitation anomalies at one half of the magnitude are contoured

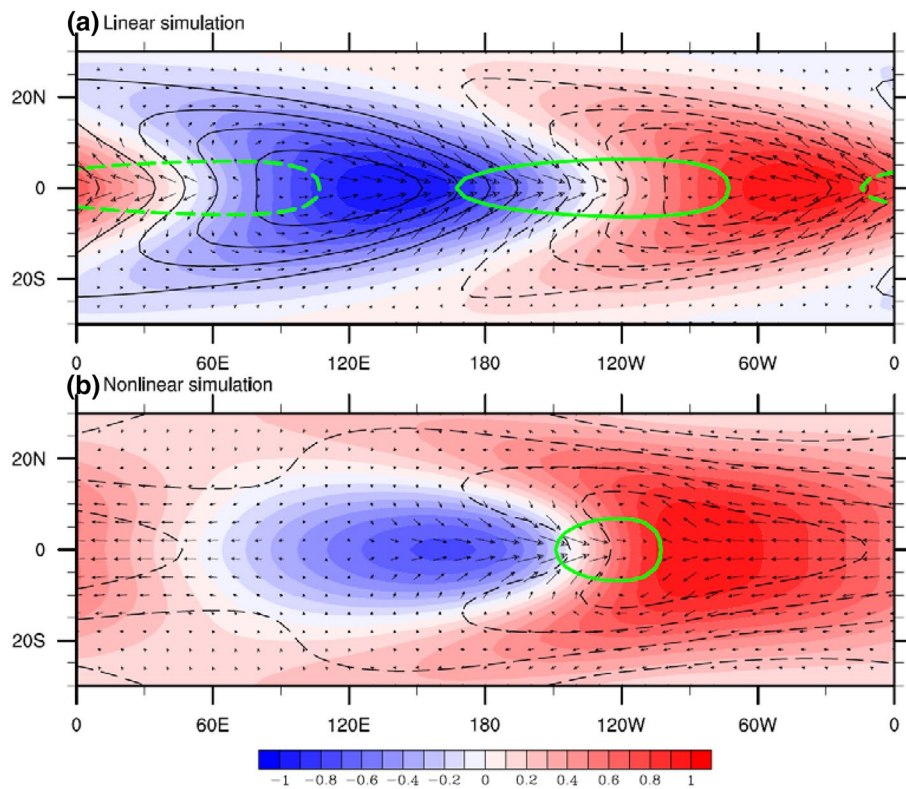
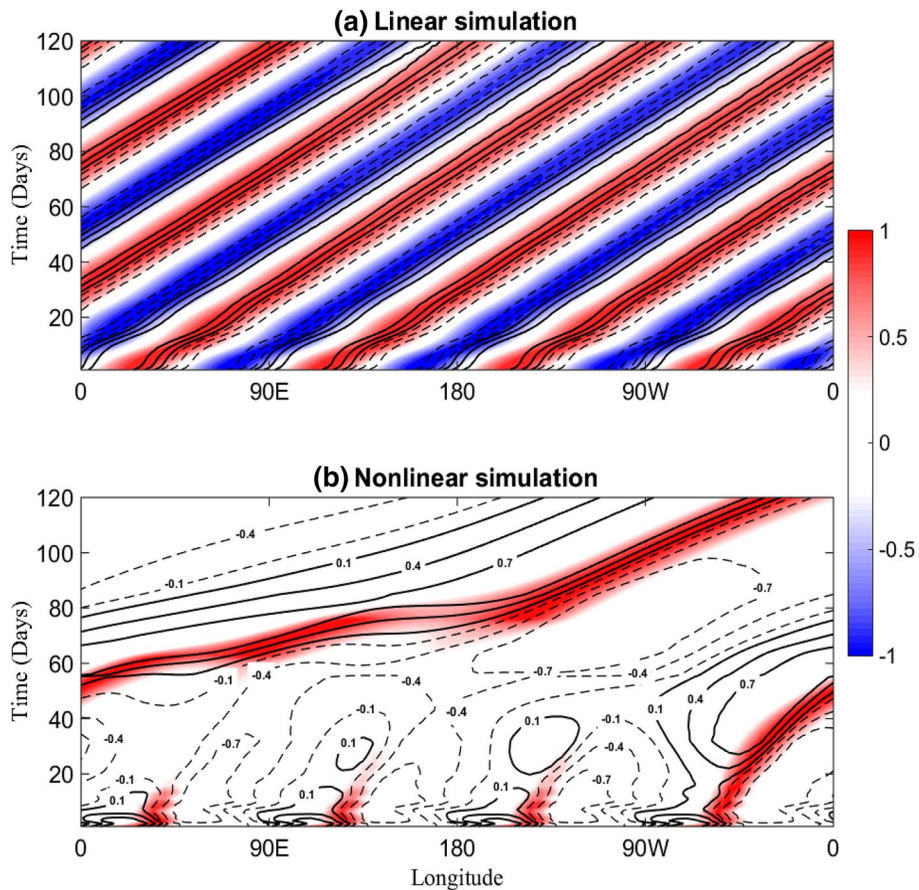


Fig. 5 Time-longitude sections of normalized low-level zonal wind (contour) and precipitation (shading) anomalies on the equator in the ASDM model with **a** linear heating and **b** nonlinear positive-only heating, in which a zonal wavenumber-four Kelvin wave-like geopotential height anomaly is used as the initial perturbation. The solid (dashed) contours denote westerly (easterly) anomalies. Contour interval is 0.3 and zero contours are not shown. Only precipitation above one third of the magnitude is shaded. All variables are normalized for each day, based on their magnitude on that day



wavenumber one has an eastward propagation with a speed of 4.0 m s^{-1} , consistent with the observed MJO.

In the linear simulation, the wavenumber-four structure is stable, and each component of the wavenumber-four system has the same amplitude (Fig. 5a). The nonlinear model gives a different simulation (Fig. 5b), in which the convective scale is relatively smaller than that in the linear model. Asymmetric evolution also exists in this nonlinear simulation, and the fourth component develops more quickly than the other three components. Since day 15, the convection from the original wavenumber four is dominated by the fourth component, and the westerly wind anomalies as well as the convergence of the other three components become weak; the first component to the east of this strongest component even disappears (keeping in mind that periodic boundary condition is used in the zonal direction). Since day 20, because the other three convective components are greatly suppressed, the circulation anomalies that are well coupled with the long-lasting convective component are strengthened quite rapidly, and only wavenumber-one anomalies can be found thereafter. This asymmetric evolution in the nonlinear model means that small-scale perturbations tend to be suppressed, and the planetary scale is then selected.

In the nonlinear simulation, precipitation is well coupled with the wavenumber-one circulation with easterly wind anomalies prevailing to the east and westerly wind anomalies to the west by day 30. Although the zonal range of the precipitation is relatively small compared to that of the observation, this coupled system can be seen to have a planetary scale.

This planetary-scale selection can also be illustrated by decomposing different wavenumbers. Figure 6 shows the time evolution of Fourier amplitudes of the geopotential height anomalies for wavenumbers one to four. Because the initial perturbation of wavenumber four is prescribed, wavenumber four has the maximum amplitude and the other waves have zero amplitude on day 0. After some days of adjustment, the waves from wavenumber one to three begin to grow quickly and wavenumber one has the fastest growth since day 9. Wavenumber four, however, decays with time. Since day 17, wavenumber one has a stronger amplitude than wavenumber four. The spectrum of simulated precipitation is also examined, and similar results have been obtained (figure not shown). Different from the circulation that has strongest wavenumber one while other wavenumbers are very weak after 10 days, wavenumbers two and three are also strong for precipitation. Wavenumber one still has the strongest amplitude for precipitation. These analyses confirm that the nonlinear ASDM model can simulate the MJO planetary-scale selection.

Figure 7 shows how this zonal wavenumber-one selection happens in the nonlinear simulation, which depicts the

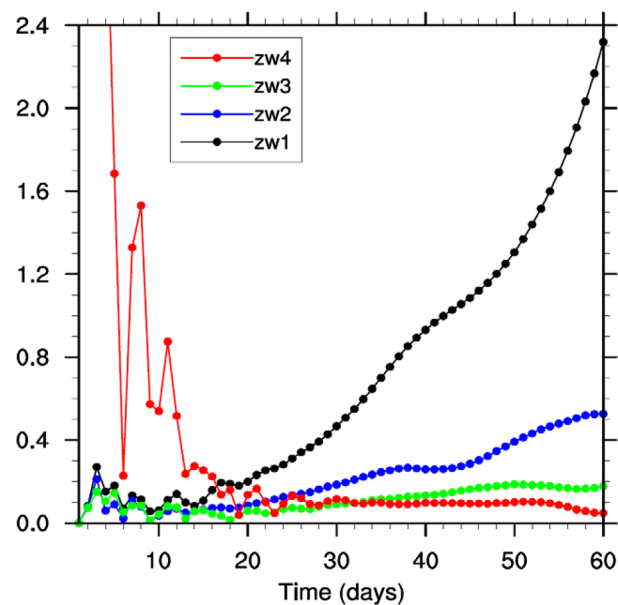


Fig. 6 Time evolution of the amplitude of low-level equatorial geopotential height anomaly for zonal wavenumber one (zw1; black), zw2 (blue), zw3 (green), and zw4 (red) by Fourier decomposition in the ASDM model with nonlinear heating. The initial perturbation is a Kelvin wave-like geopotential height anomaly of zw4

development of equatorial precipitation, low-level zonal wind, and SST anomalies from the initial wavenumber-four perturbation from day 1 to day 29 every 7 days. On day 1, each component of the wavenumber-four perturbation has the same amplitude and phase relationship. To the east of the precipitation center, the positive SST anomaly (SSTA) is led by the easterly wind anomalies. The strong negative SSTA, almost in phase with the westerly wind anomaly, lags the precipitation to the west. For each component, the negative SSTA is a little stronger than the positive one, and the westerly wind anomaly is also stronger than the easterly wind anomaly.

This symmetric structure for each of these four components, however, breaks down with time (Fig. 7). On day 15, the fourth component has much stronger precipitation anomaly than other three components. The asymmetric feature, denoted by smaller negative than positive SSTA and weaker westerly than easterly wind anomaly, becomes very strong for these three weak components. On day 29, the negative SSTA and westerly wind anomaly of the first component even disappear. It seems that the easterly wind anomaly originated from the fourth component propagates eastward and suppresses the westerly wind anomalies of other three components.

Figure 8 shows the zonal wind anomaly with the wavenumbers larger than three being removed. During the scale-selection process before day 30, the fast eastward-moving easterly wind anomaly originated from the fourth

Fig. 7 Zonal patterns of normalized equatorial precipitation (cyan shading), low-level zonal wind (blue line), and SST (red line) anomalies from day 1 to day 29, and the time interval is 7 days. The solid (dashed) lines denote positive (negative) anomalies. All variables are normalized for each day, based on their magnitude on that day

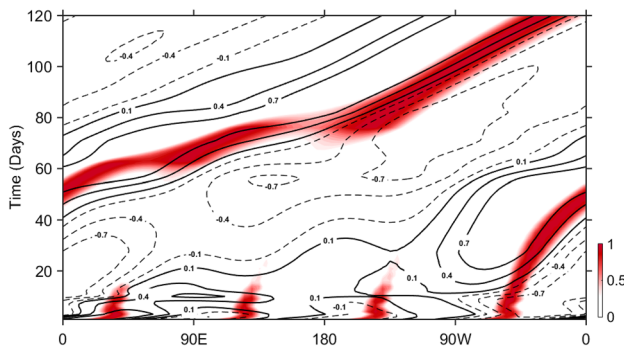
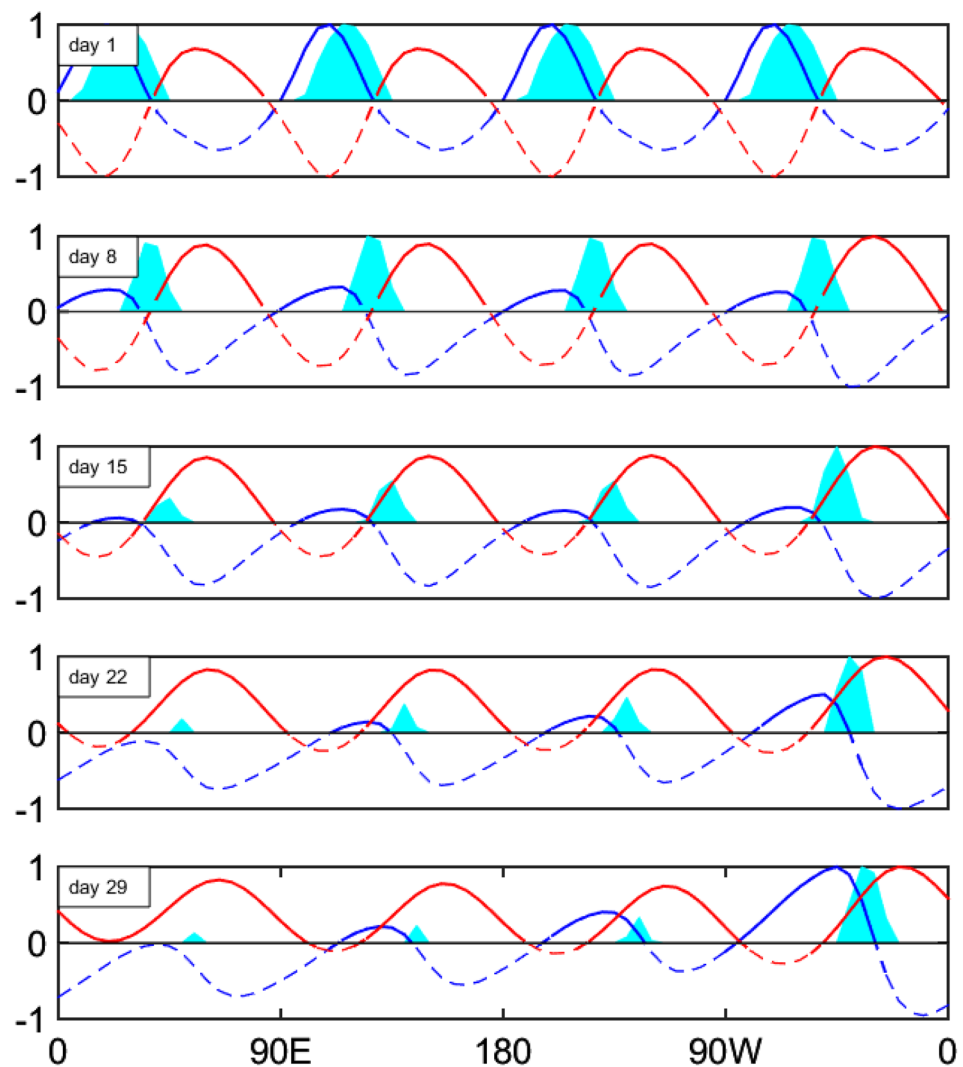


Fig. 8 Same as Fig. 5b, except that the zonal winds shown here are the anomalies in which zonal wavenumbers 4–36 have been removed

component, having a phase speed of 9.2 m s^{-1} , is clearly shown in Fig. 8, which is accompanied by largely reduced precipitation for other three weak components. It is demonstrated that the fast eastward-propagating dry Kelvin wave

from the fourth convective system does decrease the westerly wind anomaly and the moisture convergence of other sub convective systems.

On day 29 in the nonlinear simulation (Fig. 7), the westerly wind anomalies and associated negative SSTa are very weak for the three weak components, resulting in weak SST and geopotential height gradient, thus the associated wave convergence and precipitation are also reduced. Figure 9 shows the zonal pattern of equatorial SST gradient and zonal convergence on day 29. As expected, the positive SST gradient and convergence are very small for the three components on the left compared to those of the fourth component, which confirms the role of oceanic SST feedback in the MJO scale selection.

It is interesting to find the contribution of each component of these air-sea interaction processes, i.e., the wind-feedback process, the entrainment feedback, and the radiation feedback, to the planetary-scale selection. Figure 10 shows the Hovmöller diagram of the equatorial low-level

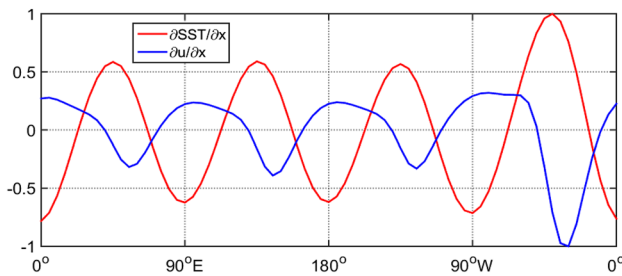


Fig. 9 Distribution of zonal gradient of anomalous equatorial SST (red curve) and zonal wind (blue curve) of day 29 in Fig. 7

zonal wind and precipitation anomalies under each of these three feedbacks. For comparison, the simulated results in the “pure” atmospheric model are also shown. We can see that the simulations with the wind-evaporation feedback (Fig. 10c) and the wind-entrainment feedback (Fig. 10d) can reproduce the scale selection, while the simulations with the cloud-radiation feedback (Fig. 10b) and the “pure” atmospheric model (Fig. 10a) cannot. Fourier analysis reveals that the “pure” atmosphere model and the simulation with the cloud-radiation feedback only present damped modes (figure not shown), and the scale selection therefore vanishes naturally. It is also worth noting that the scale selection in the wind-evaporation experiment and wind-entrainment experiment (Fig. 10c, d) is slower than that in the experiment with full air-sea interaction (Fig. 5b), since the experiment with all three processes has stronger instability than those with single air-sea interaction process.

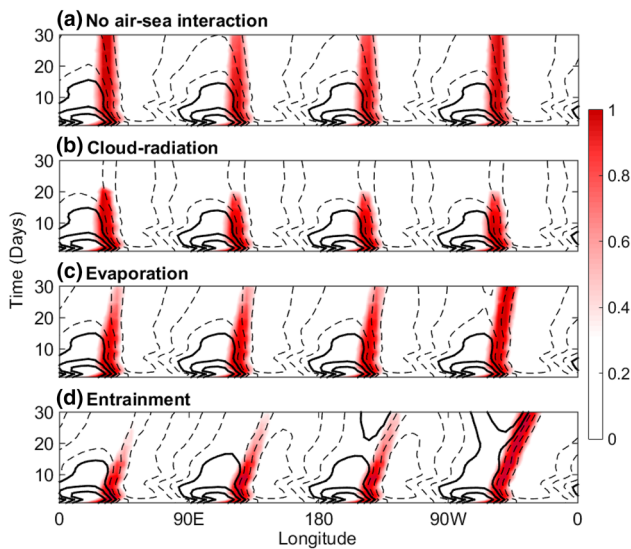


Fig. 10 Same as Fig. 5b, except for simulated results for **a** the pure atmosphere model and for the ASDM model with a single process of **b** cloud-radiation, **c** evaporation, and **d** entrainment. To focus on the scale selection, only results during the first 30 days are shown here

Previous studies (e.g., Li and Wang 1994; Wang and Li 1994; Li and Zhou 2009) showed that MJO-scale instability may arise from internal atmospheric processes in the presence of the convection-moisture-circulation feedback. Here, we demonstrate that air-sea interaction may provide an additional instability source for the MJO.

3.3 Sensitivity experiments

In the realistic free atmosphere, the dry equatorial waves should be damped in the troposphere. The Rayleigh friction and Newtonian cooling, for simplicity, are neglected in other experiments, but their roles should be discussed. In these sensitivity experiments, the time scale of 15 days is used for both Newtonian cooling and Rayleigh friction.

Figure 11a shows the Hovmöller diagram of equatorial low-level zonal wind and precipitation anomalies initiated from zonal wavenumber-four perturbation. In the nonlinear ASDM model with a damping time scale of 15 days, a slow eastward propagation of 1.3 m s^{-1} is also simulated, as in the nonlinear ASDM model without damping. It is interesting to note that the scale-selection process becomes slow when the weak damping is included. This means that the tropospheric damping should weaken the scale selection. One more sensitivity experiment with a time scale of 5 days for both Rayleigh friction and Newtonian cooling shows that the scale selection becomes weaker when the damping increases (Fig. 11b). These results indicate that the dry Kelvin waves will be suppressed under strong damping, before they can propagate far to the east to suppress the other components.

Over the tropics of the Western Hemisphere where the climatological easterly wind prevails (Wang 1988b), it is important to explore the scale selection under mean easterly wind. Figure 12 shows the time-longitude sections of equatorial low-level zonal wind, precipitation, and SST

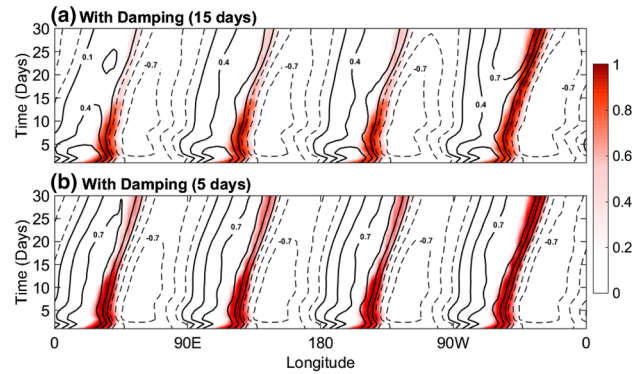


Fig. 11 Same as Fig. 5b, except for simulated results with Newtonian cooling and Rayleigh friction. The damping coefficient has a time scale of **a** 15 and **b** 5 days $^{-1}$. To focus on the scale selection, only results during the first 30 days are shown here

anomalies from the linear and nonlinear ASDM models under mean easterly wind. A slow westward-propagating (1.3 m s^{-1}) unstable mode, in which the convective center is led by the westerly wind anomalies and positive SSTa, is observed (Fig. 12a, c). All perturbations keep the initial wavenumber-four structure stably, and there is no wave selection. A much slower (0.5 m s^{-1}) westward-moving but damped mode is also simulated by the nonlinear ASDM model (Fig. 12b, d). It demonstrates that no scale selection is observed in the nonlinear simulation. Because the mode is mainly dominated by the westward-propagating Rossby waves, which are much slower than the Kelvin waves and have less effects on the nearby subconvective system. These experiments confirm the crucial importance of the mean state to the MJO dynamics.

Fig. 12 Time-longitude sections of low-level zonal wind (thin contour) and SST (red shading) anomalies on the equator for the **a** linear and **b** nonlinear simulations initiated by wavenumber-four perturbations. The solid (dashed) contours denote westerly (easterly) anomalies. Contour interval is 0.3 and zero contours are not shown. The thick blue contours represent precipitation anomalies of 0.5. All variables are normalized for each day, based on their magnitude on that day. Time evolution of maximum equatorial precipitation is also shown for the **c** linear and **d** nonlinear simulations

Different types of initial conditions are also studied (Fig. 13). For an initial wavenumber-four Rossby wave-type condition with the same geopotential height anomalies defined in Yang et al. (2003), the perturbations have a westward propagation of 4.6 m s^{-1} in the beginning (Fig. 13a). Since the precipitation associated with the Rossby waves is located in the subtropics, an average of tropical band over 10°S – 10°N is shown here. After a 10-day adjustment, the Kelvin waves are enhanced and the perturbations begin to propagate eastward slowly, with a phase speed of about 1.4 m s^{-1} . At the same time, the scale-selection mechanism works to select the fourth component to grow quickly, and the wavenumber-one coupled system forms on day 55. When the model reaches a steady-state evolution by day 80, a Gill-like horizontal structure, like the one in Fig. 4b, is

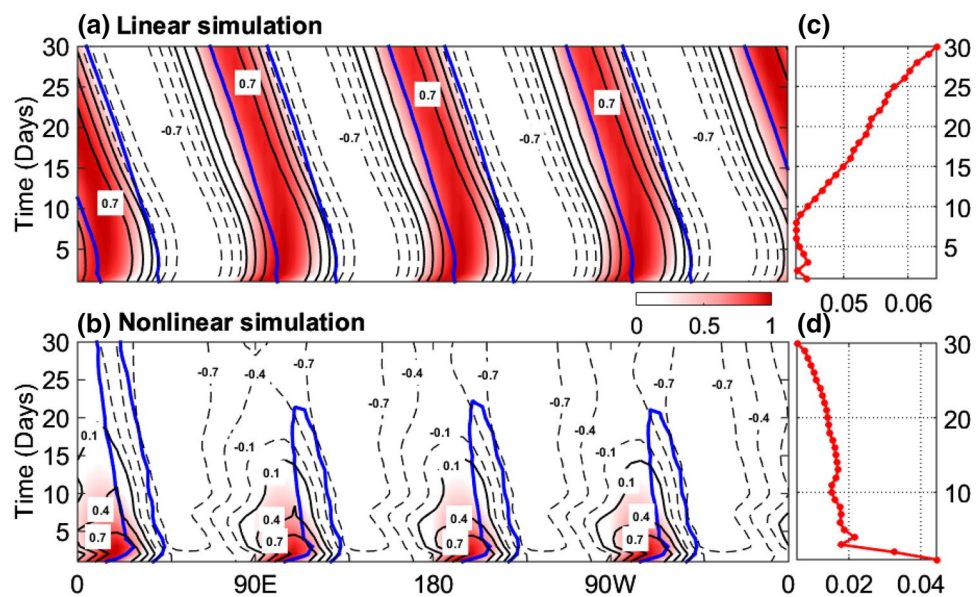
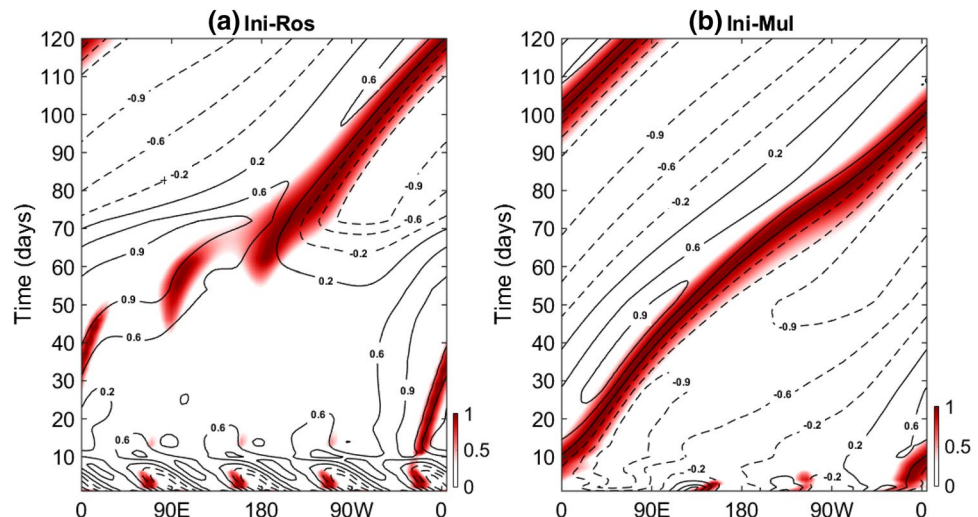


Fig. 13 Same as Fig. 5b, except for an initial perturbation **a** with a wavenumber-four Rossby wave-like structure for the geopotential height anomaly (Ini-Ros) and **b** with a multiple-wavenumber Kelvin wave-like structure comprised of wavenumbers one to four for the geopotential height anomaly (Ini-Mul), in which all wavenumbers have the same amplitude. The average of the tropical band of 10°S – 10°N is shown here



also simulated (Figure not shown). The phase speed for this steady-state period is 4.0 m s^{-1} , which is consistent with the observation. For a multiple-wavenumber initial condition comprised of wavenumber-one to wavenumber-four Kelvin wave-like geopotential height anomalies that have the same amplitude, the scale selection appears quickly and wavenumber-one perturbation is formed by day 5 (Fig. 13b), which means that the initial wavenumber-one perturbation will accelerate the scale-selection process. After the adjustment, the simulation reaches a steady state on day 80, with a slow eastward propagation of 4.0 m s^{-1} . Based on these results, more realistic initial conditions should be considered for studying the initiation of the MJO in future.

When a steady state is reached, all simulations with different initial conditions show that the longitudinal extent of precipitation anomalies is always about 20° longitude (Figs. 3b, 5b, 8, 13), which means that the model preferentially selects a horizontal scale independent of the initial condition.

We also examine the sensitivity of model solutions to the underlying mean SST (figure not shown). It turns out that for longer waves, the simulated phase speed is quite sensitive to SST in both linear and nonlinear simulations. For example, with mean SST decreasing from 30 to 25°C , the simulated phase speed of wavenumber one increases from 3.1 to 15.0 m s^{-1} in the nonlinear model. However, for shorter waves, the eastward speed is less changed when different SSTs are specified. Growth rates of longer and shorter waves are both quite sensitive to SST. Over the cold SST, the perturbations decay quickly.

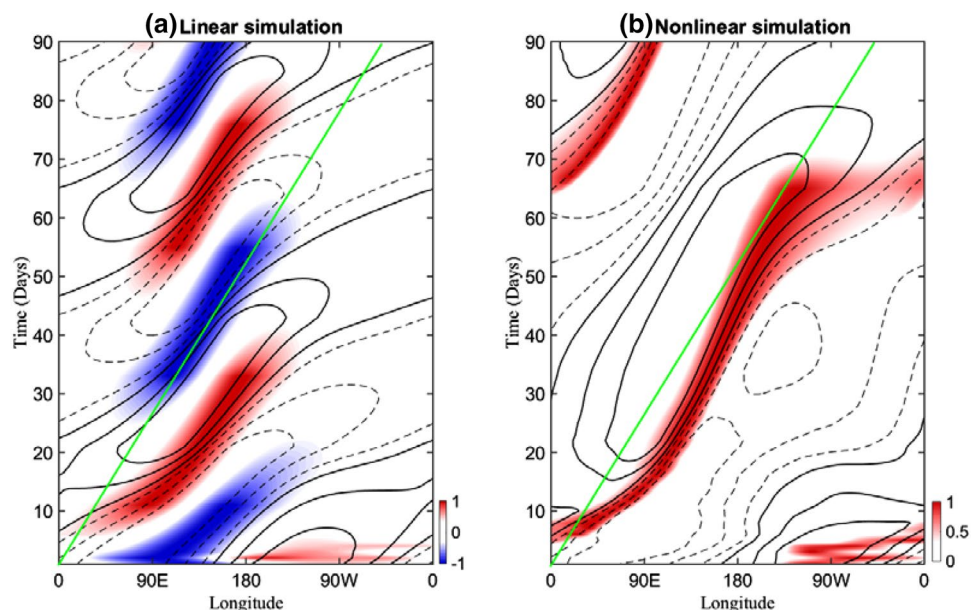
4 Results from a Warm Pool-like basic state

In the observation, the MJO convection develops and prevails right over the Indo-Pacific Warm Pool region where the underlying SST is warm. Once across the eastern edge of the Warm Pool, the convection is largely suppressed. At the same time, the anomalous circulation also decouples with MJO convection and propagates eastward fast, having a phase speed of about 15 m s^{-1} (Hendon and Salby 1994; Knutson et al. 1986). Thus, we will explore whether the ASDM model can simulate these features associated with the MJO and what the scale selection is like over a Warm Pool-like basic state. In the simulations presented here, the maximal SST over the Warm Pool region is 30°C (Fig. 1a), which is higher than the SST used in the uniform state (Sect. 3).

4.1 Simulated MJO in the ASDM model

Figure 14 shows the Hovmöller diagram of equatorial low-level zonal wind and precipitation anomalies simulated in the linear and nonlinear models, respectively, initiated from wavenumber one over the Warm Pool-like basic state. Both the linear and nonlinear ASDM models simulate the following features. Over the Warm Pool region, the eastward-moving circulation is tightly coupled with convective precipitation. The simulated propagation over the Warm-Pool region has a slow speed of 4.2 m s^{-1} (5.0 m s^{-1}) in the nonlinear (linear) simulation when the simulation reaches its steady state on day 30, which closely matches the observed phase speed of 5.0 m s^{-1} for the MJO. Over the colder ocean, however, the circulation decouples from the largely suppressed convection, and propagates eastward fast with

Fig. 14 Same as Fig. 3, except for simulation over the Warm Pool-like basic state and extended to 90 days



a speed of 9.2 m s^{-1} (15.3 m s^{-1}) in the nonlinear (linear) model.

The horizontal structures of these linear and nonlinear simulations are shown in Fig. 15. In both simulations, the convective center is located within the Warm-Pool region, and still coupled with warm SST anomalies to the east under the easterly wind anomalies and with cold SST anomalies to the west under the westerly wind anomalies. Compared to the linear simulation, the positive geopotential anomalies disappear because of lack of negative diabatic heating in the nonlinear simulation. Thus, over the Warm Pool-like mean state, the simulated evolution and structure of eastward propagating perturbations are quite close to the observed MJO features.

4.2 Planetary-scale selection over the Warm Pool-like basic state

These simulated MJOs in Sect. 4.1, which are quite close to the observations, allow us to further study the scale selection over the Warm Pool-like basic state. To better explore the scale selection over the Warm Pool region, an initial wavenumber-seven Kelvin wave-like geopotential height anomaly is used here.

Figure 16 shows the model evolution from the linear and nonlinear model simulations. Since the signals become suppressed quickly over the cold tongue region, we only

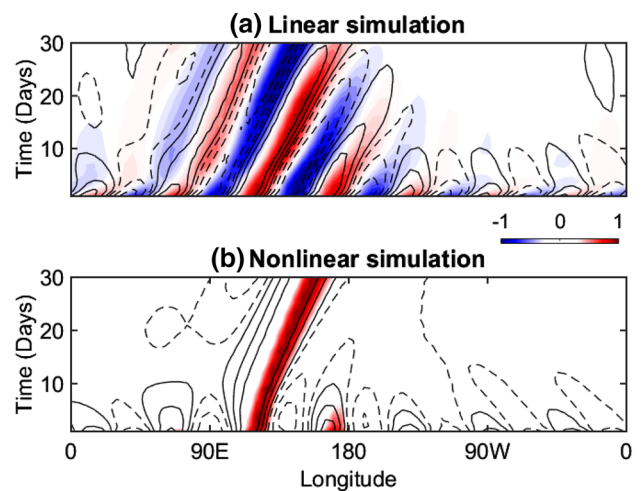
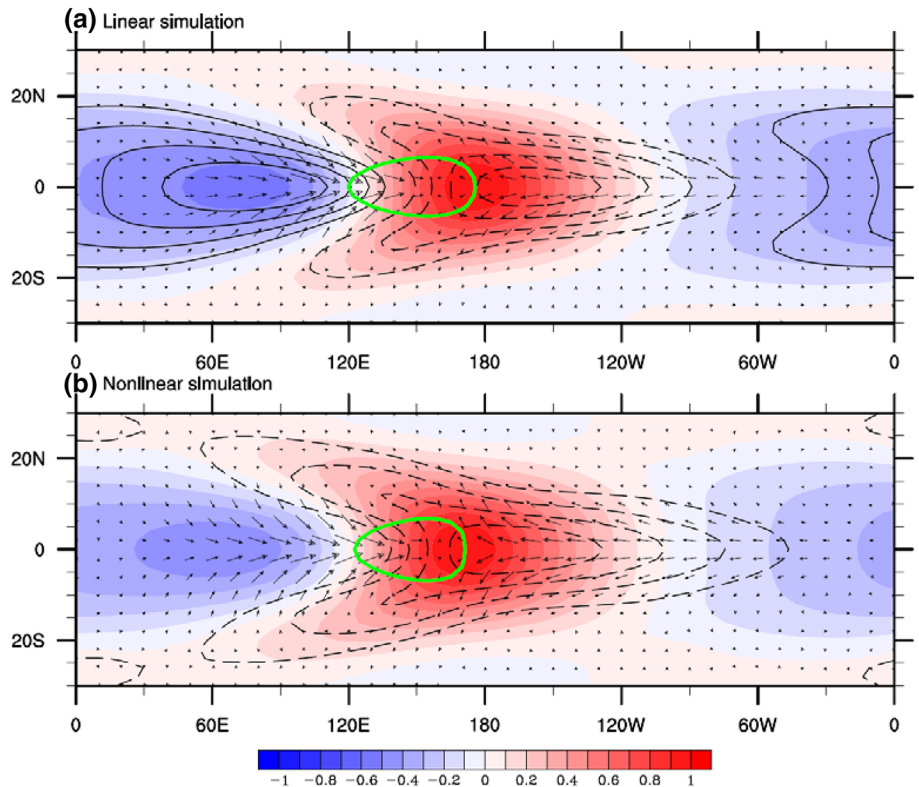


Fig. 16 Same as in Fig. 5, except for the simulation initiated from wavenumber seven over a Warm Pool-like basic state

focus on the evolution over the Warm Pool region in the first 30 days. At the initial time, two convective precipitation branches are located right over the Warm Pool region (90°E – 180°), and other five components stay over the cold region in both simulations. The moist and warm background state over the Warm Pool region provides the initial asymmetry, in which perturbations over the Warm Pool grow more strongly, while other components decay quickly

Fig. 15 Same as Fig. 4, except that a Warm Pool-like basic state is specified



in both linear and nonlinear simulations. Thus, this moist and warm Indo-Pacific region can be viewed as a natural scale-selection factor. For example, in the linear ASDM model simulation (Fig. 16a), the precipitation and low-level zonal wind are dominated by the third component over the Warm Pool region after day 15. More interestingly, scale selection tends to be accelerated in the nonlinear simulation (Fig. 16b). For instance, in the first 10 days, the fourth convective component decays quickly and disappears on day 7. In the linear simulation, however, the fourth component remains on day 10 and does not disappear before moving out of the Warm Pool region on day 15. Thus, it is necessary to examine the scale selection carefully during the first 10 days. The second component in the nonlinear simulation decays quickly because it is located over the cold ocean (Fig. 16b).

Figure 17 depicts the development of equatorial low-level zonal wind, precipitation, and SST anomalies initiated from wavenumber seven in the linear and nonlinear ASDM models over the Warm Pool-like basic state. In the linear simulation (Fig. 17a), the weak amplitude asymmetry occurs on day 1, and the perturbations over the Warm Pool are stronger than those over the cold tongue region. With time, this asymmetry becomes stronger, while there are still more than two convective centers over the Warm Pool region on day 9. In the nonlinear simulation (Fig. 17b), this asymmetry is much stronger than that in the linear simulation. From day 1 to day 3, the warm SST prefers the growth of sub components over the Warm Pool region. The wave selection mechanism caused by the positive-only heating works quickly since day 3. Five days later, there is only one convective center left over the Warm Pool region (please see day 7 in Fig. 17b). Compared to the slow selection process over the uniform SST that takes more than 30 days (Fig. 5b), the Warm Pool-like SST tends to accelerate the wave selection caused by the positive-only heating. The

faster dry Kelvin waves, generated by the strong heating selected by the Warm Pool, will propagate eastward and suppress the other sub components. This means the Warm Pool SST pattern provides a quicker process for selecting a growing convective center than the random process does over the uniform SST mean state.

Over the Warm Pool-like SST, sensitivity experiments show that the strong tropospheric damping will also weaken the scale selection and no scale selection can be found when the background winds are easterlies (figure not shown). The simulated phase speed is also SST dependent, and a warmer (colder) Warm Pool will result in a slower (faster) eastward propagation. The phase speed of the simulated wavenumber one increases from 2.0 to 4.2 m s^{-1} when the maximum SST decreases from 31.5 to 30°C .

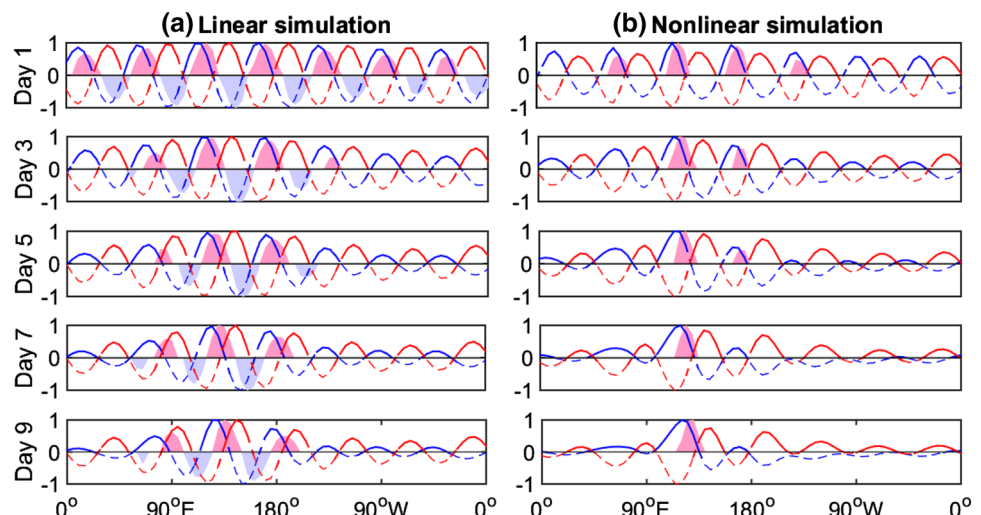
5 Summary and concluding remarks

We present an ASDM model to explore the mechanism of the preferred planetary scale of the MJO. This model is extended from the original FCDM model (Liu and Wang 2016a, b; Wang and Chen 2016; Wang et al. 2016) by coupling with an oceanic mixed-layer model (Wang et al. 1995; Wang and Xie 1998).

The main findings are summarized here.

- The nonlinear ASDM model can well simulate the observational MJO over a uniform or Warm Pool-like basic state, including (1) a planetary-scale, equatorially trapped, circulation–convection coupled, Rossby–Kelvin wave-like horizontal structure, (2) slow (fast) eastward-moving with a speed of about 4.2 m s^{-1} (9.2 m s^{-1}) and significant growing (decaying) over the Warm Pool (cold tongue) region, and (3) a phase leading of convective precipitation by positive SST

Fig. 17 Same as Fig. 7, except for the simulations initiated from wavenumber seven over the Warm Pool-like basic state. The time interval is 2 days. The purple (blue) shading denotes the positive (negative) precipitation anomaly



and easterly wind anomalies. In contrast to the linear case, the nonlinear ASDM model simulates a smaller ascending region between two much larger descending regions. The zonal range of westerly wind anomaly is much smaller than that of easterly, while the westerly wind anomaly has stronger amplitude than the easterly. These features are all consistent with previous observations and simulations (Madden and Julian 1972; Knutson and Weickmann 1987; Rui and Wang 1990; Wang and Xue 1992; Wang and Li 1994; Li and Wang 1994).

(b) Planetary-scale selection is only found in the nonlinear ASDM model with the assumption of positive-only heating. Such a scale selection cannot be reproduced in the linear model with linear heating or in the “pure” atmospheric model without other instability sources, which demonstrates that nonlinear heating is responsible for the planetary-scale feature of the MJO (Li and Zhou 2009), while the air-sea interaction can provide a new instability source to support this scale selection. The Warm Pool-like mean state can accelerate this selection process. This mechanism for the planetary scale selection of the MJO can be interpreted and summarized in Fig. 18. From initial small-scale perturbations, one sub convection will grow faster than other components through a slow random selection process, and the Warm Pool-like mean state will accelerate this selection process. Five days later the easterly wind anomalies excited from this strong component, controlled by fast eastward-propagating dry Kelvin waves, will catch up with the other slow-propagating moist sub convective systems and sup-

press their westerly wind anomalies, resulting in weak SST gradient as well as moisture convergence and precipitation. As a result, the wavenumber-one structure is selected.

(c) Sensitivity experiments show that this MJO planetary-scale selection under a stronger damping will become slower. Under mean easterly wind, no scale selection is observed in the nonlinear ASDM model, which implies the crucial importance of mean state for the MJO dynamics. Based on these model results, more realistic initial conditions should be considered for studying the initiation of the MJO in future.

This simple framework helps to add new knowledge to our understanding of the MJO dynamics in terms of air-sea interaction, and provides us a useful tool to study the air-sea interaction of the MJO, by including more complete oceanic wave dynamics that are found to contribute to the initiation of the MJO (Webber et al. 2010, 2012). In this work, the effect of SST is parameterized using a simple relationship, and the wind anomaly-induced evaporation change is not included. In numerical simulations, the strong westerly wind anomalies of the MJO were found to enhance the MJO through enhanced evaporation under the mean westerly wind (Maloney et al. 2010); and in observations, the evaporation to the east of the MJO was found to be reduced by decreased wind speed (Hsu and Li 2012). This wind anomaly-induced evaporation change mechanism should be included for more realistic MJO simulations in future. The nonlinear diabatic heating in the mid troposphere caused by SST anomalies should also be considered in future research.

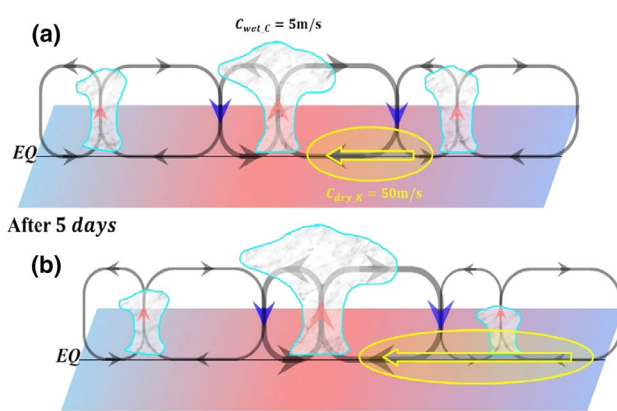


Fig. 18 Schematic diagram illustrating the scale selection of the MJO. The convective cloud is represented by gray shadings. The yellow ellipses denote the dry Kelvin waves originated from the strong component, in which the hollow yellow arrow is the dry Kelvin easterly. The anomalous ascending (descending) motion is represented by red (blue) arrow. A wider arrow means stronger convection. The light red (blue) shading denotes the warm (cold) climatological SST

Acknowledgements This work was supported by the China National 973 Project (2015CB453200), the National Natural Scientific Foundation of China (41230420), the NSFC Innovative Group Grant (41421005), the grants from the IPOVAR Project (GASI-IPOVAI-01-02, GASI-IPOVAI-02), the NSFC-Shandong Joint Fund for Marine Science Research Centers (U1406401), the Strategic Priority Research Program of the Chinese Academy of Sciences (XDA11010303), the National Natural Science Foundation of China (41420104002), and the Natural Science Foundation of Jiangsu province (BK20150907). This paper is ESMC Contribution no. 169.

References

- Adames ÁF, Wallace JM (2014) Three-dimensional structure and evolution of the MJO and its relation to the mean flow. *J Atmos Sci* 71:2007–2026
- Adames ÁF, Kim D (2016) The MJO as a dispersive, convectively coupled moisture wave: theory and observations. *J Atmos Sci* 73:913–941
- Betts AK (1986) A new convective adjustment scheme. Part I: observational and theoretical basis. *Q J R Meteorol Soc* 112:677–691

- Beets AK, Miller MT (1986) A new convective adjustment scheme. Part II: single column tests using GATE wave, BOMEX, ATEX and arctic air-mass data sets. *Q J R Meteorol Soc* 112:693–709
- Davey MK, Gill AE (1987) Experiments on tropical circulation with a simple moist model. *Quart J R Meteorol Soc* 113:1237–1269
- De Szeoce SP, Edson JB, Marion JR, Fairall CW, Bariteau L (2015) The MJO and air-sea interaction in TOGA COARE and DYNAMO. *J Clim* 28:597–622
- DeMott CA, Stan C, Randall DA, Branson MD (2014) Intraseasonal variability in coupled GCMs: the roles of ocean feedbacks and model physics. *J Clim* 27:4970–4995
- DeMott CA, Klingaman NP, Woolnough SJ (2015) Atmosphere-ocean coupled processes in the Madden–Julian oscillation. *Rev Geophys* 53:1099–1154
- DeMott CA, Benedict JJ, Klingaman NP, Woolnough SJ, Randall DA (2016) Diagnosing ocean feedbacks to the MJO: SST-modulated surface fluxes and the moist static energy budget. *J Geophys Res Atmos* 121:8350–8373
- Flatau M, Flatau PJ, Phoebus P, Niiler PP (1997) The feedback between equatorial convection and local radiation and evaporative processes: the implications for intraseasonal oscillations. *J Atmos Sci* 54:2373–2386
- Fu X, Wang B, Li T, McCreary J (2003) Coupling between northward propagating ISO and SST in the Indian Ocean. *J Atmos Sci* 60:1733–1753
- Fu X, Wang W, Lee J-Y, Wang B, Kikuchi K, Xu J, Li J, Weaver S (2015) Distinctive roles of air-sea coupling on different MJO events: a New perspective revealed from the DYNAMO/CINDY field campaign. *Mon Weather Rev* 143:794–812
- Gill AE (1980) Some simple solutions for heat-induced tropical circulation. *Q J R Meteorol Soc* 106:447–462
- Hendon HH, Salby ML (1994) The life cycle of the Madden–Julian oscillation. *J Atmos Sci* 51:2225–2237
- Hirst AC (1986) Unstable and damped equatorial modes in simple coupled ocean-atmosphere models. *J Atmos Sci* 43:606–630
- Hsu P-C, Li T (2012) Role of the boundary layer moisture asymmetry in causing the eastward propagation of the Madden–Julian oscillation. *J Clim* 25:4914–4931
- Inness PM, Slingo JM (2003) Simulation of Madden–Julian oscillation in a coupled general circulation model. Part I: comparison with observations and an atmosphere-only GCM. *J Clim* 16:345–364
- Kang I-S, Liu F, Ahn M-S, Yang Y-M, Wang B (2013) The role of SST structure in convectively coupled Kelvin–Rossby waves and its implications for MJO formation. *J Clim* 26:5915–5930
- Kiladis GN, Wheeler MC, Haertel PT, Straub KH, Roundy PE (2009) Convectively coupled equatorial waves. *Rev Geophys* 47:RG2003. doi:[10.1029/2008RG000266](https://doi.org/10.1029/2008RG000266)
- Knutson TR, Weickmann KM (1987) 30–60 day atmospheric oscillations: composite life cycles of convection and circulation anomalies. *Mon Weather Rev* 115:1407–1436
- Knutson TR, Weickmann KM, Kutzbach JE (1986) Global-scale intraseasonal oscillation of outgoing longwave radiation and 250 mb zonal wind during northern hemisphere summer. *Mon Weather Rev* 114:605–623
- Lau K-M, Peng L (1987) Origin of low-frequency (intraseasonal) oscillations in the tropical atmosphere. Part I: basic theory. *J Atmos Sci* 44:950–972
- Lau K-M, Sui C-H (1997) Mechanisms of short-term sea surface temperature regulation: observations during TOGA COARE. *J Clim* 10:465–472
- Li T (2014) Recent advance in understanding the dynamics of the Madden–Julian oscillation. *J Meteorol Res* 28:1–33
- Li T, Wang B (1994) The influence of sea surface temperature on the tropical intraseasonal oscillation: a numerical study. *Mon Weather Rev* 122:2349–2362
- Li T, Zhou C (2009) Planetary scale selection of the Madden–Julian oscillation. *J Atmos Sci* 66:2429–2443
- Li T, F Tam, X Fu, T Zhou, and W Zhu (2008) Causes of the intra-seasonal SST variability in the tropical Indian Ocean. *Atmos Ocean Sci Lett* 1:18–23
- Lim H, Lim T-K, Chang C-P (1990) Reexamination of wave-CISK theory: existence and properties of nonlinear wave-CISK modes. *J Atmos Sci* 47:3078–3091
- Lindzen RS, Nigam S (1987) On the role of sea surface temperature gradients in forcing low-level winds and convergence in the tropics. *J Atmos Sci* 44:2418–2436
- Liu F, Wang B (2012) A frictional skeleton model for the Madden–Julian oscillation. *J Atmos Sci* 69:2749–2758
- Liu F, Wang B (2013) An air-sea coupled skeleton model for the Madden–Julian oscillation. *J Atmos Sci* 70:3147–3156
- Liu F, Wang B (2016a) Effects of moisture feedback in a frictional coupled Kelvin–Rossby wave model and implication in the Madden–Julian oscillation dynamics. *Clim Dyn.* doi:[10.1007/s00382-016-3090-y](https://doi.org/10.1007/s00382-016-3090-y)
- Liu F, Wang B (2016b) Role of horizontal advection of seasonal-mean moisture in the Madden–Julian oscillation: a theoretical model analysis. *J Clim.* doi:[10.1175/JCLI-D-16-0078.1](https://doi.org/10.1175/JCLI-D-16-0078.1) (press)
- Madden RA, Julian PR (1971) Detection of a 40–50 day oscillation in the zonal wind in the tropical Pacific. *J Atmos Sci* 28:702–708
- Madden RA, Julian PR (1972) Description of global-scale circulation cells in the tropics with a 40–50 day period. *J Atmos Sci* 29:1109–1123
- Madden RA, Julian PR (1994) Observations of the 40–50 day tropical oscillation—a review. *Mon Weather Rev* 122:814–837
- Majda AJ, Stechmann SN (2009) The skeleton of tropical intraseasonal oscillations. *Proc Natl Acad Sci* 106:8417–8422
- Maloney ED, Sobel AH (2007) Idealized hot spot experiments with a general circulation model. *J Clim* 20:908–925
- Maloney ED, Sobel AH, Hannah WM (2010) Intraseasonal variability in an aquaplanet general circulation model. *J Adv Model Earth Syst* 2:1–24
- Matsuno T (1966) Quasi-geostrophic motions in the equatorial area. *J Meteorol Soc Jpn* 44:25–43
- Miura H, Satoh M, Katsumata M (2009) Spontaneous onset of a Madden–Julian oscillation event in a cloud-system-resolving simulation. *Geophys Res Lett* 36:L13802. doi:[10.1029/2009GL039056](https://doi.org/10.1029/2009GL039056)
- Philander SGH, Yamagata T, Pacanowski RC (1984) Unstable air-sea interaction in the tropics. *J Atmos Sci* 41:604–613
- Rui H, Wang B (1990) Development characteristics and dynamic structure of tropical intraseasonal convection anomalies. *J Atmos Sci* 47:357–379
- Seiki A, Nagura M, Hasegawa T (2015) Seasonal onset of the Madden–Julian oscillation and its relation to the southeastern Indian Ocean cooling. *J Meteorol Soc Jpn* 93A:139–156. doi:[10.2151/jmsj.2015-047](https://doi.org/10.2151/jmsj.2015-047)
- Sobel AH, Gildor H (2003) A simple time-dependent model of SST hot spots. *J Clim* 16:3978–3992
- Sobel A, Maloney E (2012) An idealized semi-empirical framework for modeling the Madden–Julian oscillation. *J Atmos Sci* 69:1691–1705
- Sobel A, Maloney E (2013) Moisture modes and the eastward propagation of the MJO. *J Atmos Sci* 70:187–192
- Tomasi C (1984) Vertical distribution features of atmospheric water vapor in the Mediterranean, Red Sea, and Indian Ocean. *J Geophys Res Atmos* (1984–2012) 89:2563–2566
- Waliser DE, Lau KM, Kim J-H (1999) The influence of coupled sea surface temperature on the Madden–Julian oscillation: a model perturbation experiment. *J Atmos Sci* 56:333–357
- Wang B (1988a) Dynamics of tropical low-frequency waves: an analysis of the moist Kelvin wave. *J Atmos Sci* 45:2051–2065

- Wang B (1988b) Comments on “an air–sea interaction model of intra-seasonal oscillation in the tropics”*. *J Atmos Sci* 45:3521–3525
- Wang B, Chen G (2016) A general theoretical framework for understanding essential dynamics of Madden–Julian oscillation. *Clim Dyn.* doi:[10.1007/s00382-016-3448-1](https://doi.org/10.1007/s00382-016-3448-1)
- Wang B, Li T (1994) Convective interaction with boundary-layer dynamics in the development of a tropical intraseasonal system. *J Atmos Sci* 51:1386–1400
- Wang B, Rui H (1990) Dynamics of the coupled moist Kelvin–Rossby wave on an equatorial β -plane. *J Atmos Sci* 47:397–413
- Wang B, Xie X (1998) Coupled modes of the warm pool climate system. Part I: the role of air-sea interaction in maintaining Madden–Julian oscillation. *J Clim* 11:2116–2135
- Wang B, Xue Y (1992) Behavior of a moist Kelvin wave packet with nonlinear heating. *J Atmos Sci* 49:549–559
- Wang B, Li T, Chang P (1995) An intermediate model of the tropical Pacific Ocean. *J Phys Oceanogr* 25:1599–1616
- Wang B, Liu F, Chen G (2016) A trio-interaction theory for Madden–Julian oscillation. *Geosci Lett* doi:[10.1186/s40562-016-0066-z](https://doi.org/10.1186/s40562-016-0066-z)
- Webber BGM, Matthews AJ, Heywood KJ (2010) A dynamical ocean feedback mechanism for the Madden–Julian oscillation. *Q J R Meteorol Soc* 136:740–754
- Webber BGM, Matthews AJ, Heywood KJ, Stevens DP (2012) Ocean Rossby waves as a triggering mechanism for primary Madden–Julian events. *Quart J R Meteorol Soc* 138:514–527
- Wheeler M, Kiladis GN (1999) Convectively coupled equatorial waves: analysis of clouds and temperature in the wavenumber-frequency domain. *J Atmos Sci* 56:374–399
- Yang G-Y, Hoskins B, Slingo J (2003) Convectively coupled equatorial waves: a new methodology for identifying waves structures in observational data. *J Atmos Sci* 60:1637–1654
- Zebiak SE (1986) Atmospheric convergence feedback in a simple model for El Niño. *Mon Weather Rev* 114:1263–1271
- Zhang C (1996) Atmospheric intraseasonal variability at the surface in the tropical western Pacific Ocean. *J Atmos Sci* 53:739–758
- Zhang C (2005) Madden–Julian oscillation. *Rev Geophys* 43:1–36